

TITLE: SUPRATHERMAL ELECTRON TRANSPORT
IN LASER-PRODUCED PLASMAS

MASTER

AUTHOR(S): R. J. MASON

SUBMITTED TO: To appear in the proceedings of the ANS/ENS
International Topical Meeting on "Advances
in Mathematical Methods for Nuclear Engineering
Problems", Munich, W. Germany, April 27-29, 1981.
Submitted Jan. 19, 1981.

University of California

By acceptance of this article the publisher agrees that the
U.S. Government retains a nonexclusive, irrevocable, and
exclusive right to publish or reproduce the published form of this contribution
or to allow others to do so, for U.S. Government purposes.

The Los Alamos Scientific Laboratory requests that the pub-
lisher identify this article as work performed under the au-
thority of the U.S. Department of Energy.

REPRODUCTION OF THIS DOCUMENT IS UNLIMITED



LOS ALAMOS SCIENTIFIC LABORATORY
Post Office Box 1663 Los Alamos, New Mexico 87545
An Affirmative Action/Equal Opportunity Employer



SUPRATHERMAL ELECTRON TRANSPORT
IN LASER PRODUCED PLASMAS

R. J. Mason
Los Alamos National Laboratory
Los Alamos, New Mexico 87545

A self-consistent, collisional, particle-in-cell scheme has been developed to model the one dimensional transport of suprathermal electrons in laser produced plasmas. This full Monte Carlo approach was taken, since earlier, simpler models have failed to explain an experimentally almost universal anomalous inhibition of thermal transport. The Monte Carlo scheme allows for free-streaming, ion scatter, and self thermalization of the electrons, which are moved in self-consistent E-fields computed with the aid of implicit fluid moments. PIC hydrodynamics for the ions, ponderomotive forces, and resonance and inverse-bremsstrahlung absorption of the light are all accommodated. In application to the anomalous inhibition problem, use of the scheme demonstrates that intrinsic differences in the Monte Carlo, and conventional flux-limited diffusion modelling of the transport results in apparent and real inhibition, explaining the need for strong flux-limiting in the simpler diffusion modelling of experiments.

This work was performed under the auspices of the United States Department of Energy.

SUPRATHERMAL ELECTRON TRANSPORT IN LASER PRODUCED PLASMAS

INTRODUCTION

For laser fusion applications a good electron transport scheme is essential to determine where the energy deposits in targets. From knowledge of the detailed deposition, we can then go on to determine the pellet hydrodynamics, and ultimately its thermonuclear burn performance.

This paper describes a self-consistent Monte Carlo scheme, developed over the past few years, for the transport of electrons in laser irradiated targets. The current formulation, capabilities and limits of the scheme are outlined, and demonstrated in application to transport in simple target configurations.

Electron transport is dominated by collisions in the interior of a target, where the density of background electrons exceeds $5 \times 10^{22} \text{ cm}^{-3}$, for example. However, even at such high densities an ohm's law E-field is active, drawing a return current of cold background electrons, in response to penetrating streams of hot electrons from the laser deposition sites. Nearly everywhere in pellets E-fields maintain a strong quasi-neutrality, since, generally, the transport and hydrodynamic phenomena occur on scales much larger than a Debye length λ_D . At critical density, where the light is absorbed by resonance absorption, and beyond in the corona, the principal electron transport is collisionless and dominated by E- and B-fields. At the present we avoid the B-field effects by confining our scheme to one-dimensional studies, although, in fact, the B-fields may have a most significant influence on lateral transport. An advantage of our Monte Carlo approach is that its extension to higher dimensions should be quite straightforward.

In the very earliest electron transport schemes the laser energy was deposited in a single thermal "group." The electron velocity distribution was implicitly assumed to be a skewed Maxwellian. The electron density n_e was set equal to the local ion charge density Zn_i , the flow current, $j_e = n_e v_e$, was, therefore, equal to the ion flow $j_i = Zn_i V_i$, and heat was diffused in the single electron group, in accordance with Spitzer's thermal conductivity. In long-mean-free path regions, such as the corona, where the conductivity was unphysically large, it was reduced by a flux-limiter, which would set the maximum heat flow at $q = f n v_e k T_e$, $v_e = \sqrt{k T_e / m}$, with $f = 0.6$ from free-molecular flow considerations.² Later it was found that a much smaller $f (= 0.03)$ was needed to model experiments³, a curiosity which has motivated much additional work.

For a long time it has been recognized that, in addition to heating the thermal electrons, lasers act to produce a suprathermal electron component, from the resonance absorption⁴ process, for example. Zimmerman⁵ was the first to account for this additional high energy component using multi-group diffusion. His early scheme had difficulties establishing quasi-

neutrality in the collisionless corona, however. To avoid these, we developed a two-component, double-diffusion scheme⁶, which treated both the hot and cold as flux-limited fluids, coupled by self-consistent E- and B-fields. This approach gave the first two-dimensional results for supra-thermal transport, but an adequate means for treating the evolving hot electron temperature T_h was lacking, i.e., T_h was taken as constant, and the results still depended on somewhat arbitrary flux-limiters.

To avoid these difficulties a Monte Carlo hybrid approach was developed.⁷ The supra-thermal electrons were created at the critical surface and transported by PIC-collisional Monte Carlo. The cold electrons were moved as a donor-cell fluid. However, to close the fluid equation hierarchy, we still found it necessary to employ a flux-limiter in the thermal heat conduction equation. Self-consistent E-fields were obtained by either a "plasma period dilation technique" or a "moment method", precursory to the field prescription used in the present paper. In response to incident Monte Carlo supra-thermal currents, this model gave return thermal currents⁸ that could severely limit net heat conduction in the thermals. While the implications of this result are still of interest, there remained the problem that experimentally an $f = 0.03$ limiter was required even at low laser intensities ($I < 3 \times 10^{14}$ w/cm² at 1.06 μ m), where the supra-thermally induced return currents should be weak.

Thus we have been lead to the scheme of the present paper, in which both the supra-thermals and the thermals are treated via Monte Carlo. This has been applied to the transition regime thermal heat flow, in which the background thermals are collision dominated, and the coronal thermals are nearly collisionless, i.e. effectively supra-thermal. Indeed, we find that the Monte Carlo heat flow thru pellet-like density profiles differs substantially from the classically flux-limited diffusive flow, and that the use of $f = 0.03$ can serve to bring the two descriptions into some accord.

THE FULL-MONTE CARLO APPROACH

A Monte Carlo approach has been followed, principally to provide us with the detailed electron distribution function at each position and each required instant of time. The electron motion is highly non-linear, so that the establishment of even a small charge imbalance of numerical origin (from approximations in the advancement scheme, say) can result in enormous E-fields leading to computational instability, and/or gross errors in the subsequent evolution of the system. Consequently, we cannot, for example, follow each electron singly about the mesh for many time steps, only occasionally recalculating the fields, as might be our privilege, in the case of photon or neutron transport. Instead, all the electrons must be advanced together each time step, so as to establish the new distribution function, its moments, and the new fields. We have found the interaction between the electron and ion motions to have significant bearing on the electron transport; consequently, the ions are also moved as Monte Carlo particles, although a conventional hydrodynamic treatment for the ions would, undoubtedly, suffice for most applications.

At the critical surface laser light is absorbed and supra-thermal electrons are emitted. Charge conservation is accomplished by using weighted particles, and reducing the weights of background particles, as the new emission proceeds. From the vacuum up to critical the light absorbs by inverse-bremsstrahlung. To model this, we "kick" the sub-critical electrons appropriately. Arrays for "hot" and "cold" electrons are

preserved in the code, although with the present full-Monte Carlo scheme, all the electrons are treated basically the same. Thus, as a heuristic aid, we can, for example, switch the label of an electron from hot to cold, once it has been heated.

The electrons scatter off ions and other electrons,⁷ and undergo Coulomb drag against themselves, so every cycle operators are used to modify the electron velocities accordingly. Following the velocity update from absorption and collisions, the E-fields are calculated by the implicit moment technique.⁹ Then the electrons and ions are advanced according to

$$u^{(m+1)} = u^{(m)} + \frac{q_\alpha E^{(m)}}{m} \Delta t, \quad (1a)$$

$$x^{(m+1)} = x^{(m)} + u^{(m+1/2)} \Delta t, \quad (1b)$$

where (q_α, m_α) are $(-e, m)$ for the electrons and (Ze, M) for the ions, i.e., $\alpha \equiv e, c$ and i . Here, $u^{(m+1/2)} = [u^{(m+1)} + u^{(m)}]/2$. To simplify the storage requirements, and facilitate the centering of the collision operators, all the particle and moment data are stored at full time levels - (m) . Fluid moments, $n_{h,c,i}$, $j_{h,c,i}$ and $P_{h,c,i}$, for example, are then attributed to an Eulerian mesh, via standard particle-in-cell area weighting¹⁰ procedures.

INITIALIZATION AND HEATING

Particle Loading

For a typical calculation we use 100 cells of equal size, with two external ghost cells to handle boundary conditions. Particles are loaded from left to right, with, typically, 80 electrons and 80 ions placed at each cell center in Maxwellian velocity distributions, established with the aid of a Gaussian random number generator. The particles are given weights which are normalized so that the sum of the particle densities in each cell is equal to the density profile prescribed for the problem of interest. One must be cautious in establishing density gradients larger than, say, 5-to-1 across a cell boundary, since subsequent mixing of large and small weighted particles can lead to noisy results and erroneous interpretations. Zero density cells can be established by excluding particles from such cells or by ascribing them zero weights. Care is taken throughout the code to do the physically plausible thing, should one be required to divide by zero density.

Inverse-Bremsstrahlung

Light is assumed to enter the mesh from the right. Heating can be accomplished by simply "kicking" and returning any particles crossing the right boundary and entering its ghost cell. More generally, a critical surface is declared and body heating kicking is carried out to the right of this surface. The kicking deposits energy at the desired rate by adding velocity increments to the particles, consistent with a Maxwellian at the kicker temperature $kAT_k = 3/2E$, where E is the absorbed energy/cell-cycle. The kicker can be turned off when the plasma temperature exceeds some es-

established maximum, as might be expected with inverse-bremsstrahlung.

For striator modeling the code scans from the right, locating the boundary to the right of the first over-dense cell. Then light is tracked in, absorbing via the inverse-bremsstrahlung coefficient, i.e., as $\exp(-k_I dx)$, with

$$k_I = \frac{c_1 n_e n_i z^2 g_f S_p}{(kT_e)^{1/2} \nu^3 \left(1 - \frac{n_e}{n_0}\right)^{1/2}}, \quad (2a)$$

in which $c_1 \equiv 4/3 (2\pi/3m)^{1/2} e^6 h^{-1} c^{-1}$, $\nu \equiv c/\lambda$, with λ the laser wavelength and c the speed of light, $\beta \equiv h\nu/kT_e$, $S_p = 1 - \exp(-\beta)$, and the group factor

$$g_f = \max \left[\left(\frac{3}{\pi\beta}\right)^{1/2} \left(1 - \frac{1}{4\beta}\right), g_m \right], \quad \beta > 4$$

$$= \max \left[\left(\frac{3}{\exp(\beta)}\right)^{1/2} \frac{1}{\pi} [\log \frac{4}{\beta} - 0.5772], g_m \right], \quad \beta < 4$$

where the minimum $g_m = 2(3)^{1/2}/\pi$ is obtained from the Born approximation.¹ Here, S_p corrects for spontaneous emission, and $(1 - n_e/n_0)^{1/2}$ accounts for the group velocity reduction as $n_e \rightarrow n_0$, the critical density. After a specified fraction of the energy has been dumped in the cell beyond the critical boundary, the remaining light is reflected and again deposited by k_I until it leaves the system. The deposited energy in each cell is, of course, then distributed over the particles with the kicker.

Resonance - Absorption

The dumped energy at critical can be used to heat the background electrons with the kicker, or, alternatively it can be used to emit resonance absorption suprathermals at a temperature $T_h(\text{keV}) = 30.16 [I/10^{17} \text{ W/cm}^2 (\lambda/1.06 \mu\text{m})^2 T_c(\text{keV})]^{1/3}$, $I > 10^{15} \text{ W/cm}^2$, in consistency with experiment and theory.¹¹ These electrons are usually emitted in a 2π cone towards the laser, although any emission angle can be specified. At moderate intensities for glass lasers only a small fraction of the background electrons at critical are needed to carry off the dumped energy at the high resonance absorption temperature. Thus, we found it impractical to try to draw off enough background electrons for reuse as a resonance emission distribution, and chose instead to emit totally new particles, while reducing the weights of all the background particles in the emission cell. This complicated the bookkeeping a bit, but provides much more latitude in describing the suprathermal transport.

Ponderomotive Force

The light pressure pushes on the electrons, conceivably altering their transport characteristics.¹² To model this, prior to collision, the electrons are accelerated to $u^{(m†)}$ in the ponderomotive force F according to

$$u^{(m†)} = u^{(m)} - \frac{1}{2cn_0m} \frac{\partial}{\partial x} [I^{(m)}(x) (1 - \frac{n(x)}{n_0})^{-1/2}] \Delta t .$$

Here $I^{(m)}(x)$ is the sum of the incident and reflected intensities determined during the absorption calculations. Again, the root term represents the effects of the slowing of the light group velocity near critical, n_0 .

COLLISIONAL EFFECTS

Scatter

It is assumed that an electron undergoes many small angle deflections on crossing a finite thickness of target material. Since the successive collisions are independent events, the central limit theorem indicates that for Rutherford scattering, the distribution of net deflection angles, $\theta > 0$ from the forward direction of each electron, will be approximately Gaussian,^{13,14} i.e.,

$$g(\theta) = 2(2\pi \langle \theta^2 \rangle)^{-1/2} \exp \left(-\frac{\theta^2}{2\langle \theta^2 \rangle} \right) \quad (4)$$

with $\langle \theta^2 \rangle = \frac{8\pi e^4 n_0^{-2} \Delta t n_0 Z(Z+1) \log \lambda}{3c^2} \frac{1}{2} u^2 + v^2$. Here, $c^2 = u^2 + v^2$ is the particle speed, v is its transverse velocity $v^2 = u_y^2 + u_z^2$, and $c\Delta t$ is the target distance crossed between each commutative scatter. In $Z+1$ the Z is for scattering off ions and the $+1$ accounts approximately for the scatter off electrons. In each Δt random number generators are called to pick a new θ for each electron and a new uniformly distributed azimuthal angle ϕ . Thus, if the electron velocity vector is at an angle ψ relative to the x -axis such that $\cos \psi = u/c$, it acquires a new angle ψ' , satisfying $\cos \psi' = \sin \psi \sin \theta \cos \phi + \cos \psi \cos \theta$. After a scatter through θ and ϕ from its original trajectory the new velocity components are $u' = c \cos \psi'$ and $v' = c \sin \psi'$. Overall in a scattering event the velocity vector of a particle is simply rotated and its energy conserved. When the background density is sufficiently low, or the electrons are sufficiently hot with large c values, $\langle \theta^2 \rangle \ll 1$ and the electrons are essentially undeflected during the time step.

Drag

Coulomb drag slows each electrons against all the other electrons. To model this we first reduce the electron speeds by

$$\Delta c = \frac{-4\pi e^4}{mkT_e} \Delta t G(\xi) \log \lambda, \quad \xi = \left(\frac{mc^2}{2kT_e}\right)^{1/2}, \quad (5a)$$

in which

$$G(\xi) = \frac{0.376 \xi}{(1 + 0.542 \xi - 0.504 \xi^2 + 0.752 \xi^3)} \quad (5b)$$

is a polynomial fit to Sptizer's error function combination.¹⁴ For $\xi \gg 1$, $G(\xi) \sim kT_e/(mc^2)$ and eq. (5a) goes to eq. (5a) of ref. 7. However, for lower speeds $G(\xi)$ peaks roughly at 0.2 for $\xi = 1$, and $G(\xi) \rightarrow 0$ when $\xi \rightarrow \infty$. Within each cell the drag process should be momentum and energy conserving, so the energy lost to drag is redeposited isotropically in the original drift frame of the electrons by the usual kicking procedure. The net drag operator drives all the electrons to a local Maxwellian, while affecting the slowest and fastest electrons least.

As formulated, these procedures treat collisions accurately, only so long as $v(c)\Delta t \equiv 1/2 \langle \theta^2 \rangle < 1$. Thus, in practice, for the calculations of θ , θ is either truncated at unity or replaced by $\theta + 2 \arctan(\theta/2)$, which varies smoothly from 0 to π as $\theta \rightarrow 0 \rightarrow \infty$. In regions where $v(c)\Delta t \gg 1$, diffusion should apply, and Monte Carlo free-streaming of the electrons by eq. (1b) results in excessive excursions for the particles that ignore the brownian character of the motion during the many large-angle collisions in the interval Δt . Similarly, the drift in E from eq. (1a) will be an overstatement. A guaranteed cure for these difficulties is to switch to a fluid description for the collisional electrons in such regions, as accomplished in ref. 7. Alternatively, a form of flux limiting for the Monte Carlo is under consideration, by which eq. (1b) would be replaced by

$$x^{(n+1)} = x^{(n)} + \frac{u^{(n)} \Delta t}{[1 + (v(c)\Delta t)]^{1/2}} - eE^{(n)} \frac{(\Delta t)^2}{m[1 + v(c)\Delta t]}$$

This should effect brownian diffusion and ohm's law drift when $v(c)\Delta t \gg 1$, and classical streaming between collisions in the more traditional $v(c)\Delta t < 1$ Monte Carlo limit.

THE IMPLICIT E-FIELD

The E-field is obtained by the implicit moment method.⁹ This frees us from the need to calculate on the local plasma frequency, $\omega_p = 4\pi e^2 n_e/m$, time scale. The method uses the fluid moments accumulated each cycle from the particles to predict the densities \tilde{n} that will prevail, as a function of E, at the end of the next time step. These densities are put in Poisson's equation, which is then solved implicitly for the new predicted \tilde{E} . The predicted field is then taken to be $\tilde{E}^{(n+1)}$ and the particles are accelerated in the centered field $E^{(n+1)} = (\tilde{E}^{(n+1)} + E^{(n)})/2$.

Thus, in the absence of collisions, from the momentum equations we get⁹

$$j_{\alpha}^{(m+1/2)} = j_{\alpha}^{(m)} - \frac{1}{m_{\alpha}} \left[\frac{\partial p_{\alpha}^{(\dagger)}}{\partial x} - q_{\alpha} n^{(\dagger)} E^{(\#)} \right] \frac{\Delta t}{2} \quad (7a)$$

Here, $j_{\alpha} \equiv n_{\alpha} v_{\alpha}$, and $p_{\alpha} \equiv n_{\alpha} (kT_{\alpha} + m_{\alpha} U_{\alpha}^2)$ is the second moment over particles, i.e., $m \Sigma u^2$. This is used with continuity

$$\tilde{n}_{\alpha}^{(m+1)} = n_{\alpha}^{(m)} - \frac{\partial}{\partial x} (j_{\alpha}^{(m+1/2)}) \Delta t \quad (7b)$$

and the integrated Poisson equation,

$$\tilde{E}^{(m+1)} = 4\pi \int_0^x \sum_{\alpha} q_{\alpha} \tilde{n}_{\alpha}^{(m+1)} dx + \tilde{E}^{(m+1)}(0) \quad (7c)$$

Solving the eq. (7), assuming $E(0) = j(0) = 0$ for a quiescent or symmetric left boundary we obtain

$$\tilde{E}^{(m+1)} = \frac{4\pi \int_0^x \sum_{\alpha} q_{\alpha} n_{\alpha}^{(\pi)} dx - \sum_{\alpha} q_{\alpha} j_{\alpha}^{(m)} \Delta t + \sum_{\alpha} \frac{q_{\alpha}}{m_{\alpha}} \frac{\partial p_{\alpha}^{(\dagger)}}{\partial x} \frac{(\Delta t)^2}{2} - \frac{\omega_p^2 (\Delta t)^2}{4} E^{(\pi)}}{1 + \frac{\omega_p^2 (\Delta t)^2}{4}} \quad (8)$$

in which,

$$\omega_p^2 = \frac{4\pi e^2}{m} (n_e^{(\dagger)} + \frac{m}{M} Z^2 n_i^{(\dagger)}) (\Delta t)^2$$

we have found it sufficient to use $n^{(\dagger)} = n^{(m)}$ and $p^{(\dagger)} = p^{(m)}$, as long as the time step is confined to a Courant condition $\Delta t < \Delta t_{\text{Courant}} = \Delta x / (|U_h| + \sqrt{kT_h/m})$. Somewhat larger time steps are permitted with $p = n^{(\#)}$ and the "isothermal" $p^{(\dagger)} = n^{(\#)} kT^{(m)}$ or "adiabatic" assumptions $p^{(\dagger)} = p^{(m)} (n^{(\#)}/n^{(m)})^{\gamma}$, using $n^{(\#)} = Zn_i^{(m)} - 1/4\pi e \partial E^{(\#)}/\partial x$ and iterating eq. (8) to convergence.

In the quasi-neutral limit $\omega_p \Delta t \gg 1$, which is of primary interest for laser fusion, when the ion are motionless ($M \rightarrow \infty$), eq. (8) rearranges to give

$$E^{(*)} = \frac{\tilde{E}^{(m+1)} + \tilde{E}^{(m)}}{2} = \frac{-2m \left\{ \int_0^x n_\alpha^{(m)} dx - j_\alpha^{(m)} \Delta t + \sum \frac{1}{n_\alpha} \frac{\partial \alpha^{(*)}}{\partial x} \frac{(\Delta t)^2}{2} \right\}}{en_e^{(*)} (\Delta t)^2} \quad (9)$$

When the $\int n_\alpha^{(m)}$ and $\sum j_\alpha^{(m)}$ "correction terms" are neglected, eq. (9) reduces to the familiar form $E^{(*)} = -1/en_e^{(*)} \sum \partial \alpha^{(*)} / \partial x$. If there is a lack of quasi-neutrality in the present cycle, the correction terms give E-field components that will act to correct this imbalance in the next cycle.⁹

Denavit¹⁵ and others¹⁶ have suggested an altered centering for the field, eq. (9), and for the particle eqs. (1), that can act to damp out the highest frequency plasma waves. We, however, have favored centered formulations of the implicit moment method for overall energy conservation, particularly in transport applications. In practice, to insure stability we do introduce a little damping by using $E^{(*)} = \theta \tilde{E}^{(m+1)} + (1-\theta)E^{(m)}$, $\theta = 0.55$, for example, and modifying eqs. (8) and (9), accordingly. Also, for effective centering, it is necessary to project the particles to their positions at half-time, when sampling the $E^{(*)}$ for eq. (1a).

The effects of source heating and collisions on the E-field are included by accumulating the $\alpha^{(*)}$ after these processes, and by the substitutions

$$j^{(m)} \rightarrow j^{(m')} = j^{(m)} + \frac{\partial j}{\partial t} \Big|_{s,c} \frac{\Delta t}{2} \quad (10)$$

in which $\partial j / \partial t \Big|_{s,c} = (j^{(m*)} - j^{(m)}) / \Delta t$ and $j^{(m*)}$ is accumulated following the heating and collisions. Thus, $j^{(m')} = (j^{(m)} + j^{(m*)}) / 2$, because of the centering employed. Without this centering the $\sum j_\alpha^{(m)} \Delta t$ correction term in eqs. (8) and (9) can rapidly cool the plasma in strongly collisional regions, due to an interplay of fluctuational currents created by the collisions process, and the E-fields responding to drive these currents to zero. However, strong scattering tends to reverse current fluctuations, i.e., $j^{(m*)} = -j^{(m)}$, so with the eq. (10) centering $\sum j_\alpha^{(m')} \Delta t$ tends to zero, improving the energy conservation.

Eventually, for improved calculations in the strongly collisional regime, in conjunction with the use of eq. (6), we anticipate that the mean collision operator in eq. (7) will be made implicit, so that for electrons

$$j_\alpha^{(m+1/2)} = j_\alpha^{(m)} + \dots - \frac{en_\alpha}{m} E^{(*)} \frac{\Delta t}{2} - \nu_\alpha' j_\alpha^{(m+1/2)} \frac{\Delta t}{2} \quad (11)$$

where ν_α' is a suitable mean collision frequency.⁷ Then the currents should go properly to their ohm's law values, $j_\alpha^{(m+1/2)} = -en_\alpha^{(m)} E^{(*)}$, when $\nu_\alpha' \Delta t \gg 1$.

ADDITIONS

Pending additions to the model are: (a) the inclusion of a circuitry capability to permit the study of charged elements in targets, and specifically, an examination of fast electron bleed-off from target atmospheres and (b) the implimention of ion-ion self collisions, as performed for the electron drag, to allow studies of ion counter-streaming coupling, and ion-beam target interactions.

APPLICATIONS

The transport of resonance absorption suprathemals, $T_h > 20$ keV, has been treated extensively with the hybrid Monte Carlo code of ref. 7. the present fully Monte Carlo model was developed chiefly to explore the transport of mildly suprathemal electrons, produced at from 1 to 4 keV by the inverse-bremsstrahlung process. It appears that the new model is now sufficiently complete, so that from the results of its application to a number of simple test problems, we can finally construct an explanation for the anomalous transport inhibition of thermal electrons.

AN END-HEATED UNIFORM PLASMA

As an initial application we looked at the transition regime $\lambda_{mfp}/L = 1$ transport configuration, recently investigated by T. Bell et al.⁷ at the Rutherford laboratories. They simulated by Fokker-Planck a uniform plasma heated at one end to four times its background temperature, $T_h/T_c = 4$. In Bell's study the hot electron mean-free-path was 16 computational cells, and the cold $\lambda_{mfp} = \Delta x$. The Rutherford workers found that a flux limit factor, $f = q/(mhn_a^3)$, $v_a = \sqrt{kT_a/m}$, of 0.1 was established in their simulations, at the point of maximum temperature gradient. Here T_a is the local mean temperature of electrons in the plasma. For example, $T_a = (n_h T_h + n_c T_c)/(n_h + n_c)$, if colds are changed to hots upon entering the heating region.

Our results for the same problem are collected in Fig. 1. All the frames are for 2.9 ps ($= 2.9 \times 10^{-4}$ shakes) after the heating was initiated in the 6 cells to the right of the vertical fiducial. A total of 100 cells was employed with $\Delta x = 0.24 \mu m$. The ions are held motionless. Frame (a) plots $n_e = n_h + n_c$ and Zn_1 . We took Z to be 10 for SiO_2 , the Rutherford workers used $Z = 4$. Although the electron density is allowed to vary, the implicit E-field obviously locks $n_e = Zn_1$, and no significant fluctuations from the initial $n_e = 10^{21} cm^{-3}$ is evident, even near the heating region. We allowed the kicker to heat the electrons to an average of 1.7 keV in the heating region, should the temperature rise above this level for a cycle, the heater was shut off. Frame (b) shows that a potential $\theta = - \int_0^x E dx$ of ~ 2.7 keV has been established in the heating region, capable of trapping electrons at $2.7/1.7 = 1.6$ times T_h -- and drawing in the required cold return current. Frame (d) shows the phase space of heated particles. Their thermal spread is obviously greater in the heating region. particles striking the left wall were returned to the plasma with positive velocities in a Maxwellian distribution at the initial background temperature 0.43 keV.

Finally, from frame (c) we extract the significant results. It gives both the Monte Carlo results, and results at the same time from a piggy-back, single-group, flux-limited diffusion calculation -- for comparison. That is, the energy deposited into the M.C. particles recorded, and the same energy is sourced into the parallel diffusion calculations each cycle.

Thus, at 2.9 ps we get two temperature profiles, the smoother one is for flux-limited diffusion for $f = 0.3$, the wiggly T_h curve is for the Monte Carlo. We also plot the local effective $f_e \equiv |q|/(m\nu_a^3)^{-1}$, where $q = q_{MC} = \Sigma m\nu_a^3$ for the Monte Carlo, and $q = q_d = q_u/[1 + |q_u|/(f m\nu_a^3)^{-1}]$, $q_u \equiv -k \partial T_a / \partial x$, for the diffusion. These are essentially the normalized heat fluxes. Note that the flux-limiter is introduced as a harmonic mean; we have not investigated the case where it is imposed as an absolute maximum.

With $f = 0.3$ the Monte Carlo and limited diffusion temperatures agree in the heating region, so do the normalized heat fluxes f_e ($\equiv f_d$ and f_{MC}) neighboring the heater. The effective f_e is lower at the heater, ~ 0.2 , due to the smooth way the limitation is introduced. When stronger limitation is employed, e.g. for $f = 0.1$, the coronal diffusion temperature is mismatched and climbs to 3.0 keV. With $f = 0.5$ this temperature drops to 1.3 keV. In each of these cases the heater boundary f_e values fail to match, as well. Thus, to match coronal temperature, f should be 0.3. However, in the body of the plasma at 2.0 ps the diffusion temperature is much too high near the heater. The fundamental problem is that the limited diffusion front advances thru the material with the form of a non-linear heat wave, while the Monte Carlo heating penetrates much like a free-streaming expansion. The first profile is convex, the second concave. At any time the diffusion profile stores significant heat behind its front that the Monte Carlo profile has sent a head from the distribution tail as suprathermals. Thus, one can conclude, the diffusion profile will heat less matter near the kicker to higher temperatures than will the Monte Carlo profile. Hence, the diffusion profile should lead to higher radiation emissions, and increased ablation. To bring the two temperature profiles into accord in the body of the plasma, one could increase f , at the expense of a temperature mismatch in the corona. Historically, experiment has manifested too much emission and ablation with $f = 0.6$. This simulation indicates that the problem has derived from the inability of the flux-limited diffusion to mock-up the detailed character of the transition region thermal flow.

We note that these conclusions are essentially unchanged when the simulations are performed in the absence of scatter and drag. In this case an $f = 0.5$ is needed to match the coronal temperatures and heater-boundary heat flux. Again, a much larger f is required to match the temperature profiles in the body of the plasma neighboring the heater.

HOT CORONAL PREDOMONANCE

As a second application we look at transport thru a density jump. The previous problem is modified by raising the density to $n_e = 3 \times 10^{21} \text{ cm}^{-3}$ for $x < 12.1 \mu\text{m}$, turning off the scatter and drag, and thickening the heating regions. The ions are still fixed.

Figure 2 shows the results after 11.9 ps. Frame (a) plots Zn_i , n_e and n_h . A cold electron is converted to a hot electron upon being kicked in the heating region. A potential rise develops at the density drop. The density of heated electrons drops about 50% across the jump. This is also evident in the phase plot, frame (d), which shows only the hot electrons. Here, frame (c) displays just the temperature profiles. The diffusion curve is for $f = 0.6$. By 11.9 ps the diffusion profile is nearly flat thru the density jump, while the Monte Carlo temperature profile sustains the 1.7 keV driving temperature to the right of the jump, and drops essentially to the diffusion temperature to its left.

This simulation leads us to two important observations. (a) First, in a two component collisionless system of hots and colds, the hots tend to dominate the lower density corona, i.e., in the corona $T_e = T_h$. In the denser interior there will be a mixture of hots and colds, so that for a large density jump and a moderate temperature difference the interior temperature will be $T_e = (n_h T_h + n_c T_c) / n_c = T_c$. Thus, at the interface there can be a large temperature jump, but no necessity for heat flow. The temperature gradient is sustained by the small potential required to keep the colds in the high density region. In such a configuration $q = -K \partial T_e / \partial x$ simply fails to apply at such an interface, although a desired temperature gradient can be established with the use of an appropriate flux-limiter. (b) It is more difficult than has been generally believed to draw a significant return current down thru a density gradient. With body heating, nearly half the low density electrons are kicked into the high density region. The return current must drift thru a "field-filter" which returns most of the high density electrons to the left and accelerates the remaining few to the right at \sim half the low number density to the hot electron speed. If the filtered incident colds fail to reach the hot speed, they cannot supply the required return current, and some hots will be inhibited, retained and recycled in the heating region. Thus, frame (b) shows a significant accelerating (negative) E-field at the density interface, and the development of the 0.8 keV potential, retaining some hots, to its right. We note that the restoration of scattering and drag to these calculations, smears the temperature and potential curves somewhat, but leaves these conclusions invariant.

ION MOTION EFFECTS

An E-field develops to draw a return current: (a) into body heating, e.g. inverse-bremsstrahlung, regions, and (b) down thru density gradient regions. On the ion times scale these fields act to lower the density in body heating regions and at the foot of density ramps. This is evident from the Fig. 3 results. Frame (a) shows the Zn_1 profile after 2.9 ps, under the conditions for Figs. 1 and 2, but with scattering and drag "off" and the ions permitted to move, but with a reduced mass ratio, such that $M_n/m_e = 100$, with M_n the mass of a nucleon. (Thus, in fact, this motion would not occur until $(1836/100)^{1/2} \times 2.9 \text{ ps} = 12.4 \text{ ps}$.) The critical surface has been arbitrarily placed at $18.2 \mu\text{m}$ to separate the body heating, and density gradient effects. Clearly, the density has been decreased to $0.6 \times 10^{21} \text{ cm}^{-3}$ by the return current fields. Frame (b) shows that a negative E arises at the two interfaces and that the potential rises in two steps to 6 keV. Frame (c) shows the diffusion and Monte Carlo temperatures differing in the now familiar sense, and frame (d) plots the cold (unkicked) electrons showing their tendency to achieve high velocities to produce the necessary current at low densities. Thus, the field for a return current exerts a ponderomotive-like effect at density gradients, acting to steepen them. Similarly, the body heater produces a ponderomotive-like thermal force that steepens the density profile at its boundary. The latter effect does not arise in single fluid limited diffusion treatments, which assume that the necessary source of thermal electrons for heating is always available. We note that these ion motion reductions in the density will tend to amplify the apparent and real inhibition effects observed with Figs. 1 and 2.

DUMPALL HEATING

An important observation comes from the comparative heating study that produced Fig. 4. Frames (a) and (b) show the density and temperature configurations at 4.6 ps, when the energy is deposited by body heating up to critical, which is here calculated by the code for 1.06 μm light. The density has started to drop below critical where the boundary of the body heater merges with the density gradient. The Monte Carlo temperature is twice the diffusion value in the corona, while the $f = 0.6$ diffusion profile has become flat. Frames (c) and (d) give the result, but for an earlier time, 1.9 ps, when all the energy is dumped by kicking the thermals at critical into a Maxwellian distribution. As usual, a cold electron is given the hot label as it is kicked, and hots can be re-kicked. In this case the Monte Carlo energy flows freely in both directions -- with the differences between the Monte Carlo and $f = 0.6$ diffusion temperatures being essentially those of Fig. 1. We see that the body heated (e.g., inverse-bremsstrahlung) energy is truly inhibited by the fields drawing a return current, while energy deposited below critical, as from resonance absorption, freely penetrates, aided by the relatively larger supply of return current carriers.

ABLATIVE HYDRODYNAMICS FROM INVERSE-BREMSSTRAHLUNG

In order to study the combined consequences of these effects, the Fig. 5 simulations were performed. The energy was absorbed by inverse-bremsstrahlung up to critical; the classical ponderomotive force was off. Initially, the plasma was established with an upper density of $5 \times 10^{21} \text{ cm}^{-3}$, and $0.7 \times 10^{21} \text{ cm}^{-3}$ as the lower shelf density, absorbing the energy. As the associated illumination proceeds, the dense region is gradually heated and expands. The fields associated with expansion tend to cancel the fields working to draw the return current. Frames (a) and (c) are for Monte Carlo electrons for frame (b) and (d) we heated a single $f = 0.6$ diffusion group of electrons, for which $n_e = Zn_i$, with the ions accelerated by $E = -(en_e)^{-1} \partial(n_e T_e) / \partial x$, as in conventional hydro-codes. The results are for 7.2 ps after the start of illumination, with $M_n/m = 100$. The diffusion results are from runs with f values between 0.6 and 0.01. The diffusion fiducial is for $f = 0.6$.

Comparing the two solutions, we see that under Monte Carlo the critical surface has been pushed back substantially below the $f = 0.6$ diffusion location. The Monte Carlo solution shows much less matter heated to high temperatures. Also, the diffusion coronal temperature best matches the Monte Carlo temperature for $f = 0.03$. These results are, at least, in qualitative agreement with the experimental findings that have encouraged the use of a severe flux-limiter. Thus, it appears that these many differences in the diffusion and Monte Carlo descriptions collectively explain the anomalous limitation.

CONCLUSIONS

Our full Monte Carlo approach has been shown to provide an effective tool for electron transport analysis. With it we have shown that apparent and real thermal inhibition results from the fundamental differences inherent in single-group flux-limited diffusion and Monte Carlo models, for thermals heated to long range, suprathreshold energies.

REFERENCES

1. L. G. Spitzer, *Physics of Fully Ionized Gases*, John Wiley, New York (1962).
2. R. J. Mason and R. L. Morse, *Phys. Fluids*, 18, 814 (1975).
3. R. C. Malone, R. L. McCrory, and R. L. Morse, *Phys. Rev. Lett.* 34, 721.
4. D. W. Forslund, J. M. Kindel, and K. Lee, *Phys. Rev. Lett.* 39, 284 (1977).
5. G. Zimmerman and W. Kruer, *Comments in Plasma Phys. and Controlled Fusion* 2, 85 (1975).
6. R. J. Mason, *Phys. Rev. Lett.* 42, 239 (1979).
7. R. J. Mason, *Phys. Fluids* 23, 2205 (1980).
8. R. J. Mason, *Phys. Rev. Lett.* 43, 1795 (1979).
9. R. J. Mason, submitted to the *J. of Comp. Phys.*, August 1980, and LASL Report LA-UR-79-3460 (Aug., 1980).
10. R. L. Morse, in *Methods of Computational Phys.*, edited by B. Alder, S. Fernbach and M. Rotenberg (Academic, New York, 1970), Vol. 9, p. 213.
11. D. W. Forslund, J. M. Kindel, and K. Lee, *Phys. Rev. Lett.* 39, 385 (1977).
12. R. L. Berger and T. V. Powers, *Proceedings of the 9th Annual Conference on Anomalous Absorption of Electromagnetic Waves*, Rochester, NY, May 1979, paper B-4.
13. J. D. Jackson, *Classical Electrodynamics* (Wiley, New York, 1962), p. 457.
14. ref. 1, p. 129. Polynomial fit provided by Dr. R. Jones, LASL.
15. J. Dehavit, submitted to *J. C. P.*, and Lawrence Livermore Laboratory Report UCRL-85097, (Nov. 1980).
16. C. K. Birdsall, *Proceedings of the Meeting on target time steps*, Berkeley, CA, Dec. 1980.
17. A. R. Bell, R. G. Evans and D. J. Nicholas, *Rutherford Laboratory Report*, RL-80-049 (Aug., 1980).

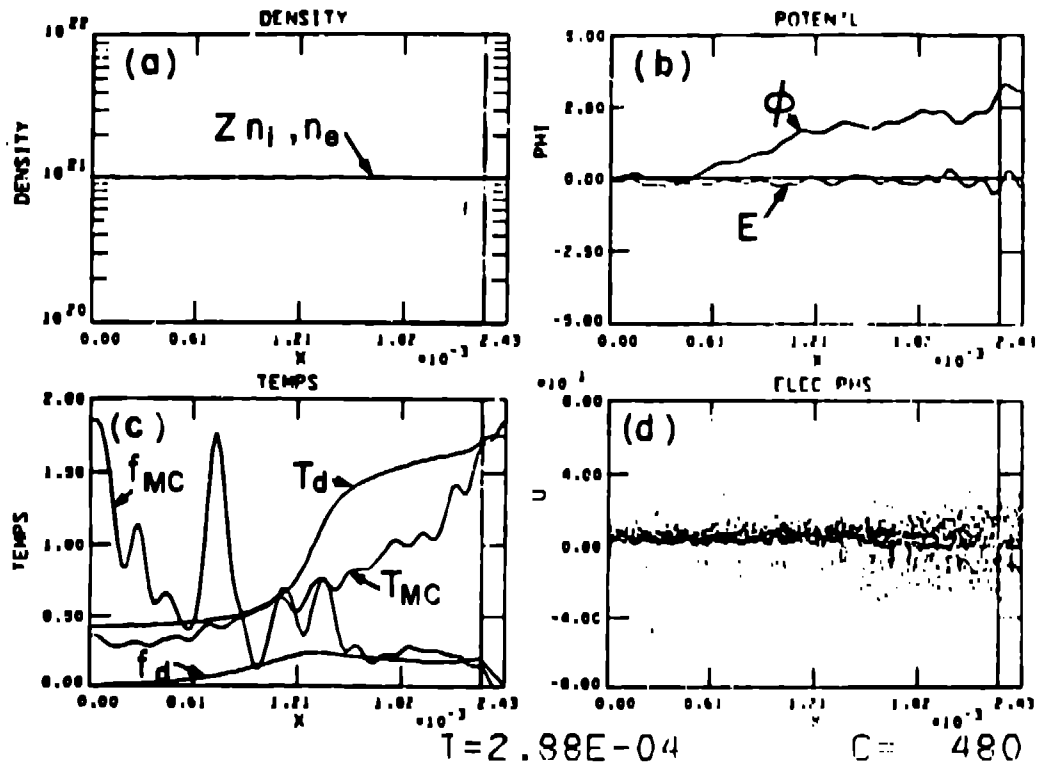


Fig. 1 An end heated uniform plasma.

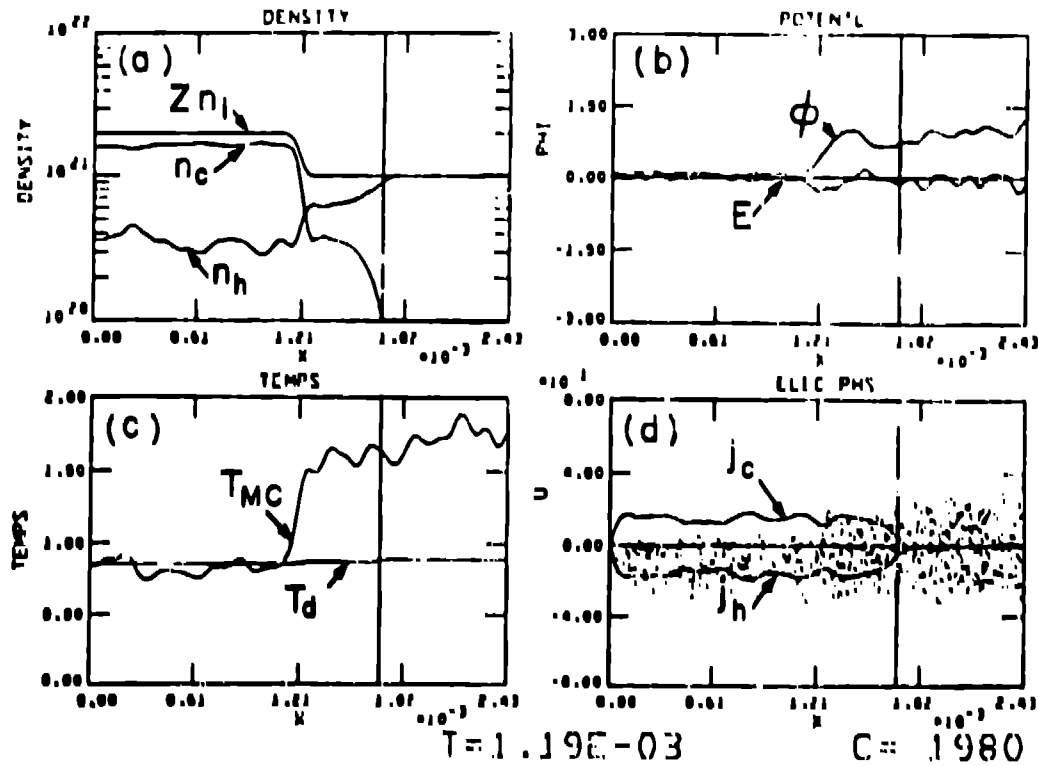


Fig. 2 Predominance of heated electrons in the corona.

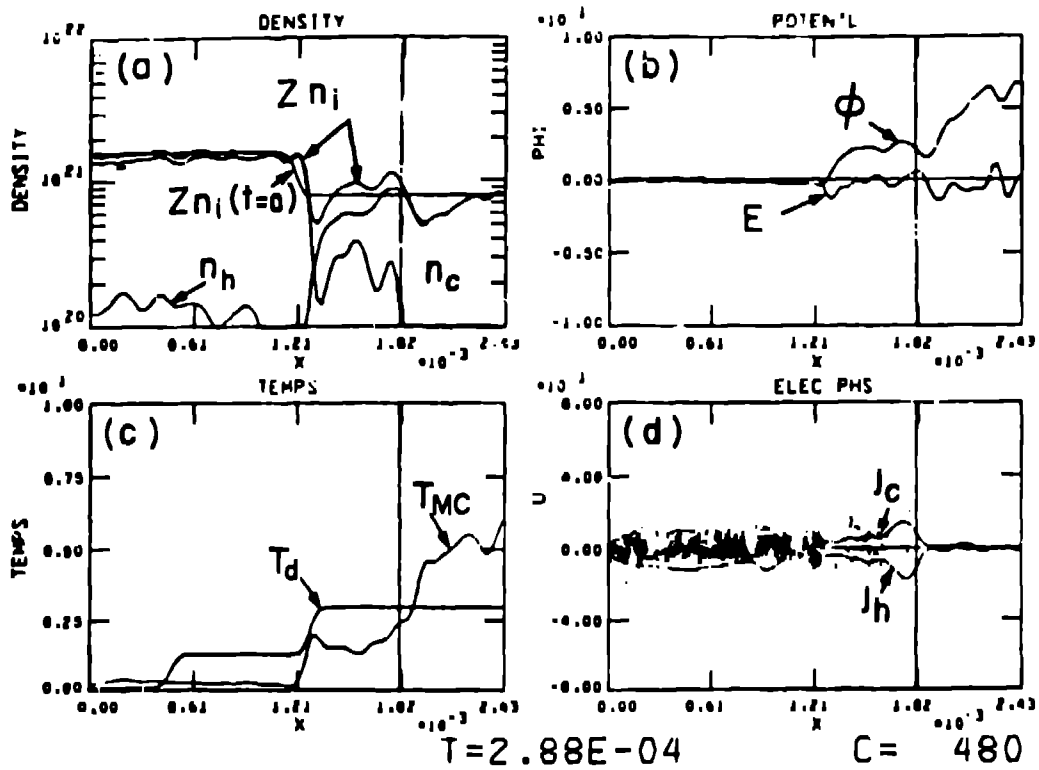


Fig. 3 Formation of density troughs at the foot of density gradients and at the edge of body heating regions

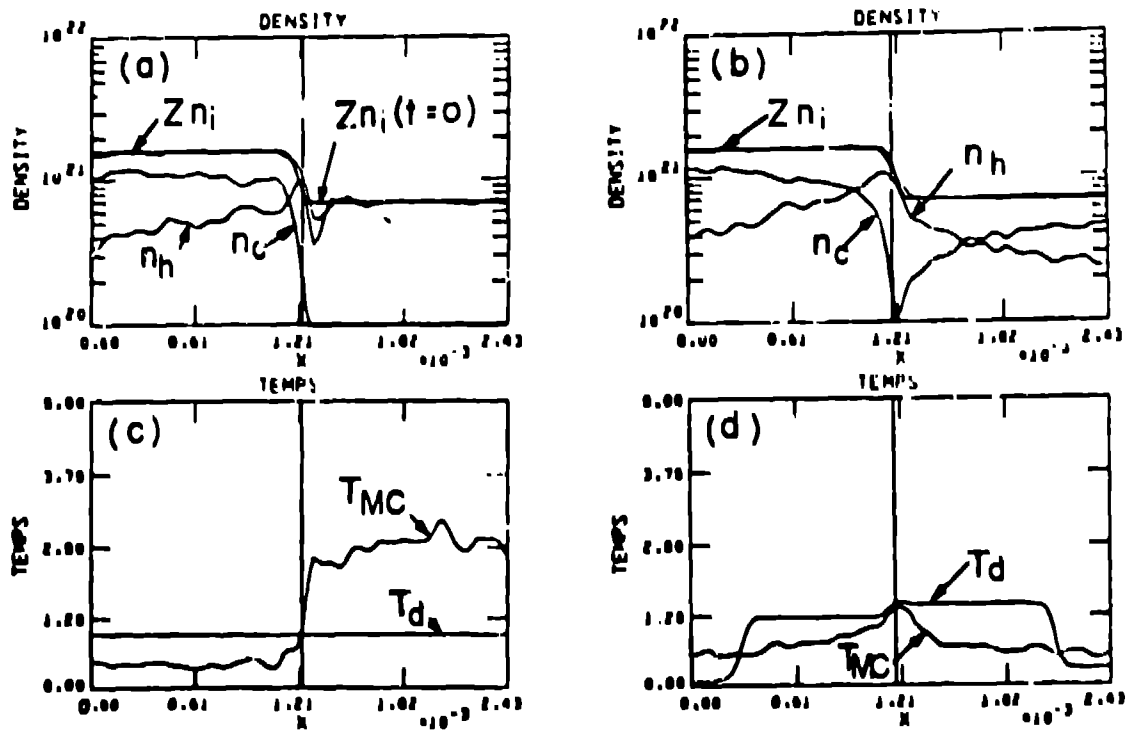


Fig. 4 Comparison of transport for energy deposited by body heating and dumpall.

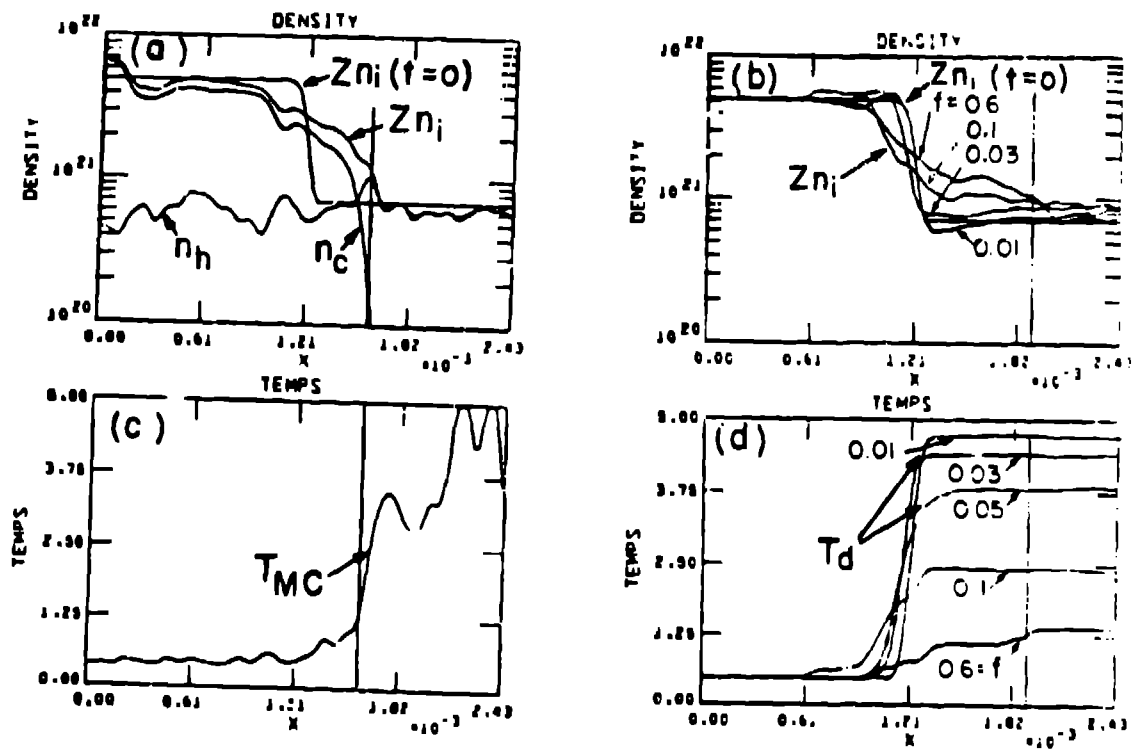


Fig. 5 Ablation calculated via Monte Carlo, and via flux-limited diffusion.